

High rate of gravitational waves mergers from flyby perturbations of wide black-hole triples in the field

Erez Michaely^{1*}, Hagai B. Perets²

¹*Astronomy Department, University of Maryland, College Park, MD 20742*

²*Physics department, Technion - Israel Institute of Technology, Haifa, Israel 3200002*

Accepted XXX. Received YYY; in original form ZZZ

ABSTRACT

Ultra-wide triple black-holes (TBHs; with an outer orbit $> 10^3$ AU) in the field can be considerably perturbed by flyby encounters with field stars by the excitation of the outer orbit eccentricities. We study the cumulative effect of such flybys, and show them to be conducive for the production of gravitational-wave (GW) sources. Flyby encounters with TBHs can turn the TBHs unstable and follow chaotic evolution. This leads to a binary-single resonant encounter between the outer BH and the inner-binary. These encounters can result in either a prompt GW-merger of two of the TBH components during the resonant phase, or the disruption of the TBH. In the latter case a more compact binary is left behind, while the third BH escapes and is ejected. The compact remnant binary may still inspiral through GW-emission, although on longer timescales. A significant number of these would lead to a delayed GW-merger in less than a Hubble time. We find a volumetric merger rate of $\sim 3 - 10 \text{Gpc}^{-3} \text{yr}^{-1}$ contributed by the (former) prompt-merger TBH channel and $\sim 100 - 250 \text{Gpc}^{-3} \text{yr}^{-1}$ contributed by the (latter) delayed-merger TBH channel. The prompt channel gives rise to eccentric mergers in the aLIGO band, while the majority of the delayed-GW mergers are circularized when enter the aLIGO band. We find the total eccentric volumetric merger rate to be $\sim 1 - 10 \text{Gpc}^{-3} \text{yr}^{-1}$ from both channels. We expect these mergers to show no significant spin-orbit alignment, and uniform delay time distribution.

Key words: Keyword – Keyword – Keyword

1 INTRODUCTION

The third observational run (O3) of the aLIGO and VIRGO consortium identified numerous gravitational-wave (GW) events, the majority of which are binary black-hole (BBH) mergers. Over the past decades a large body of theoretical studies was done in order to identify the evolutionary channels leading to the mergers of two compact objects and predict (before the LIGO era) and currently explain the observed rate of mergers and their properties Belczynski et al. (e.g. 2002, 2004, 2007, 2008, 2016); Antonini & Perets (e.g. 2012); Dominik et al. (e.g. 2012); Antognini et al. (e.g. 2014); Antonini et al. (e.g. 2014); de Mink & Belczynski (e.g. 2015); Petrovich & Antonini (e.g. 2017, and more). In the second observational run (O2) 11 GW mergers have been detected by aLIGO and VIRGO. These include 10 mergers of binary black-holes (BBHs)

and a single merger from a binary neutron-star (NS). All of the detection were consistent with zero eccentricity The inferred BBH-merger rate from O2 (in the local Universe) is $R_{\text{BBH}} = 9.7 - 101 \text{Gpc}^{-3} \text{yr}^{-1}$; while the merger rates of binary neutron-star is $R_{\text{BNS}} = 110 - 3840 \text{Gpc}^{-3} \text{yr}^{-1}$; and the upper limit of BH-NS merger is $R_{\text{BHNS}} < 600 \text{Gpc}^{-3} \text{yr}^{-1}$ (LIGO Scientific Collaboration & Virgo Collaboration 2019).

Four main evolutionary channels were proposed in the context of GW mergers. The first deals with collisional mergers in dense environments such as galactic centers or globular clusters (e.g. Rodriguez et al. 2016, 2018; Fragione & Kocsis 2018; Banerjee 2018; Hamers et al. 2018; Leigh et al. 2018; Samsing et al. 2014), where binary mergers are catalyzed by strong interactions with stars in these dense environment. In such environments, strong binary-single and binary-binary interactions lead to harden compact binaries (drive them to shorter periods) and excite their eccentricities. Such

* E-mail: erzmichaely@gmail.com

models predict GW-production rates in the range of $2 - 20 \text{Gpc}^{-3} \text{yr}^{-1}$.

The second evolutionary channel deals with the isolated evolution of initially massive close binary stars (e.g. [Belczynski et al. 2008, 2016](#); [Dominik et al. 2012, 2015](#)). In this scenario massive close binaries strongly interact through one or two common envelope phases in which the interaction of a star with the envelope of an evolved companion leads to its inspiral in the envelope and the production of a short period binary. A fraction of the post-CE binaries are sufficiently close to merge via GW emission within a Hubble time. A different merger path is through the “chemically homogeneous channel” ([Mandel & de Mink 2016](#)). The large uncertainties in the initial conditions of the binaries, the evolution in the common-envelope phase, the natal-kick experienced by NS/BHs at birth; and the mass-loss processes of massive stars give rise to a wide range of expected GW-sources production rates in the range $\sim 10^{-2} - 10^3 \text{Gpc}^{-3} \text{yr}^{-1}$.

The third evolutionary channel is mergers induced by secular evolution of triple systems either in the field (e.g. [Antonini et al. 2016, 2017](#); [Sillsbee & Tremaine 2017](#)) or in nuclear cluster and/or massive clusters (e.g. [Antonini & Perets 2012](#); [Petrovich & Antonini 2017](#); [Samsing & D’Orazio 2018](#); [Hoang et al. 2018](#); [Fragione et al. 2019](#); [Hamilton & Rafikov 2019](#)). In this channel the secular and/or semi-secular perturbations by a third companion (Lidov-Kozai evolution [Lidov \(1962\)](#); [Kozai \(1962\)](#); semi-secular evolution [Antonini & Perets \(2012\)](#)) can drive BBHs into high eccentricities such that they merge within a Hubble-time; the rates expected in this channel are $\sim 0.5 - 15 \text{Gpc}^{-3} \text{yr}^{-1}$.

The fourth channel ([Michaely & Perets 2019](#)) is from wide binaries in the field ($\text{SMA} > 1000 \text{AU}$) perturbed by flyby encounters, following similar ideas regarding formation of clue stragglers through stellar mergers of wide binaries studied by ([Kaib & Raymond 2014](#)). We found that the frequent interactions with random stars can change the eccentricity of wide binaries, and in some cases excite sufficiently high eccentricities, leading to the merger of the binary via GW emission before the next flyby happens. The predicted rate from this channel, for spiral galaxies, is $\sim 1 - 10 \text{Gpc}^{-3} \text{yr}^{-1}$. Here we follow up and extend this channel to study flyby perturbations of wide triples in the field. One of the important properties of GW mergers, that can potentially distinguish between the different channels is the eccentricity of the merged binary in the aLIGO / VIRGO band. With current observatories only eccentricities greater than ~ 0.1 at GW frequency of $\sim 10 \text{Hz}$ ([Harry & LIGO Scientific Collaboration 2010](#)) are detectable and termed as “eccentric mergers”. Currently an eccentric merger have not been detected yet, and it is important to understand all evolutionary paths that may lead to an eccentric merger and their expected rate. It was suggested that eccentric mergers are rare among mergers of isolated binaries, but that dynamical interaction in dense environments (e.g. [Samsing et al. 2014](#); [Rodriguez et al. 2016](#)) could give rise to a non-negligible rate of eccentric mergers.

Another observable property of GW-merges is the measured spin-alignment. Current observations suggest a preference for either an isotropic spin distribution or low spin magnitudes for the observed systems ([Will 2014](#)). Dynamical

channels are expected to have isotropic spin orientations, while isolated binaries channels are more likely to have spins that are preferentially aligned with the orbit. As we briefly discuss below, the TBH channel is likely to produce an isotropic distribution (with some possible caveats), more similar to the dynamical channels.

Finally, with the expectations of much more data from the coming runs of aLIGO, the delay-time distribution (DTD) of GW mergers could also become an important constraining property. The DTD presents the rate of events since the formation of BHs or essentially star formation. The mergers time of BBHs can span from years ([Michaely & Perets 2018](#)) up to Hubble time, with different channels suggesting different DTDs.

In this manuscript we expand our understanding of the fourth channel, and extend it to the study of dynamical interactions of wide triples in the field (*not* in dense stellar environments). We calculate the GW merger rate from this channel, characterize the expected eccentricity distribution, and discuss the expected spin-alignment from the channel.

The paper is structured as follows: in section 2 we briefly describe the interaction of wide TBH systems in the field and calculate the rate of these system becoming unstable due to flyby interactions. In section 3 we describe the dynamics of unstable triples and calculate the resulting galactic GW-merger rate and the rate of eccentric GW mergers. In section 4 we compute the corresponding cosmological merger rate observable by LIGO. We discuss our results in Section 5 and summarize (section 6).

2 WIDE TRIPLES IN THE FIELD

In the following we describe the dynamics of wide triples perturbed by random flyby of stars in the field. A more extended mathematical description of some of the aspects of such interactions can be found in our previous papers [Michaely & Perets \(2016, 2019\)](#). In what follows we highlight the main aspects of the mathematical model and key differences of this work focusing on wide triples compared with ([Michaely & Perets 2019](#)) where we studied wide binaries. We first describe the interaction qualitatively, subsection 2.1 following with a quantitative treatment in subsection 2.2.

2.1 Qualitative description

Several studies ([Kaib & Raymond \(2014\)](#); [Michaely & Perets \(2016, 2019\)](#)) showed that the cumulative interactions of wide systems ($a \gtrsim 1000 \text{AU}$) with field stars through flyby encounters can considerably change their (outer-orbit) pericenter distances, mainly through the excitation of the wide-binary eccentricity, somewhat similar to the case of stars interacting with massive black holes in galactic nuclei ([Lightman & Shapiro 1977](#); [Merritt 2013](#)). A fraction of these system might interact tidally [Michaely & Perets \(2016\)](#) or inspiral through GW emission ([Michaely & Perets 2019](#)). Here we focus on wide triple-BHs (TBHs) in hierarchical configurations, where, for simplicity we consider only equal-mass BHs. In such triples, the inner binary consists of two components of masses, m_1 and m_2 , with the inner orbital parameters; inner semi-major

axis (SMA) and inner eccentricity denoted by a_1 and e_1 , respectively, where, for simplicity we consider only inner binaries with e_1 set to zero (which might be expected at least for the relatively more compact binaries, if they evolved through a common-envelope evolution phase). The third BH, m_3 and the inner binary (center of mass) serve as the outer binary of the triple with the outer SMA denoted by a_2 , where we only consider cases where $a_2 \gg a_1$. For illustration see Figure 1.

We note that in this manuscript we are neglecting Lidov-Kozai effects and the effects of mass-loss on such secular evolution (Lidov 1962; Kozai 1962; Naoz 2016; Michaely & Perets 2014) because we are focusing on wide systems with $a_2 > 1000\text{AU}$. For these systems the Lidov-Kozai timescale is

$$\tau_{\text{LK}} \approx \frac{P_2^2}{P_1} \approx \quad (1)$$

$$4.7 \cdot 10^{12} \text{yr} \left(\frac{a_2}{10^4 \text{AU}} \right)^3 \left(\frac{a_1}{0.1 \text{AU}} \right)^{-\frac{3}{2}} \left(\frac{M}{30 M_\odot} \right)^{-1} \left(\frac{M_b}{20 M_\odot} \right)^{\frac{1}{2}}$$

where $M \equiv m_1 + m_2 + m_3$ is the total mass of the TBH and $M_b \equiv m_1 + m_2$ is the total mass of the inner binary, and τ_{LK} is typically much larger than a Hubble time, although it could affect TBHs of wider inner binaries and/or closer outer binaries (the latter however, would be less affected by flyby encounters discussed here). **In future work we intend to explore the regime where the two timescales overlap and potentially flybys might excite Lidov-Kozai oscillations.** For these wide systems a flyby can change the eccentricity of the outer binary such that the pericenter distance, $q = a_2(1 - e_2) \lesssim a_1$. Namely, the third BH passes within the inner binary SMA, effectively giving rise to a strong binary-single encounter, and a chaotic evolution of the now unstable triple. In this case the binary-single encounter resembles the binary-single encounters occurring in dense cluster environments, with similar expected outcomes as those studied in that context (e.g. Heggie (1975); Hills (1975); Samsing et al. (2014); Stone & Leigh (2019) and references therein). In other words, perturbed wide field triples provide an effective channel of converting isolated field evolution to a cluster-like dynamical interaction.

There are two relevant timescales for this part of the model. First, the interaction timescale, $t_{\text{int}} \equiv b/v_{\text{enc}}$, between the TBH and the flyby field star, where b is the closest approach of the flyby to the triple system and v_{enc} is the velocity at infinity of the flyby with respect to the triple center of mass. Second, the outer binary orbital period, P_2 . We restrict ourselves to the impulsive regime where $t_{\text{int}} \ll P_2$. In the next section 2.2 we calculate the rate of turning hierarchical triples into unstable triples as a function of the inner SMA.

A fraction of all systems that undergo a dynamical instability phase, $f_{\text{merger}}(a_1)$, merge during the resonant interaction phase; we term this the prompt-merger channel (see section 3.1.1), while the majority are disrupted, with one of the BH ejected, and the other two forming a typically more compact remnant binary. Some of these can later inspiral through GW emission and merge in less than a Hubble time; we term this channel for GW-sources the delayed-merger channel. For both channels we consider the expected

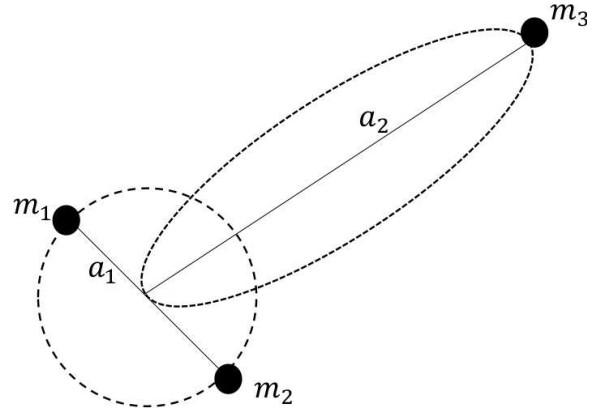


Figure 1. Illustration of hierarchical TBH system, $a_1 \ll a_2$. The inner binary is circular while the eccentricity of the outer binary is distributed with thermal distribution, $f(e_2) = 2e_2$.

rates, and characterize the expected eccentricity distribution in the LIGO band, and the fraction of eccentric mergers, $f_{\text{eccentric}}(a_1)$. We find $f_{\text{merger}}(a_1)$ and $f_{\text{eccentric}}(a_1)$ in section 3.1.1.

2.2 Quantitative description

As mentioned earlier, here we briefly review the loss-cone analysis used to estimate the TBH destabilization rates due to flyby encounters. A more detailed discussion of the loss-cone analysis in this context can be found in our previous papers.

Consider a large ensemble of wide TBHs. All BH masses are taken to be equal $m_1 = m_2 = m_3 = 10M_\odot$ (total mass is denoted by M) the inner SMA a_1 and outer SMA a_2 . The distribution of a_1 is log-uniform, $\propto 1/a_1$ and outer binary SMA $a_2 > 10^3\text{AU}$. The inner binary is set to be circular, $e_1 = 0$ while the eccentricity distribution of outer binary is assumed to be thermal, $f(e)de = 2ede$. The ensemble is embedded in the field, where the stellar number density is given by n_* and the typical velocity dispersion, σ_v , is set to be the relative encounter velocity, v_{enc} .

In the following we derive the fraction of the ensemble that sufficiently interacts with the flyby field stars such that the pericenter of the outer binary passes within the inner binary SMA, namely $q \leq a_1$, potentially a conservative assumption as triple could be destabilized even at larger pericenter separations (e.g. Mardling & Aarseth (2001)). We find the fraction dependence on the outer SMA, a_2 and field number density, n_* . Moreover, we account for outer binary ionization from the random interaction with flyby stars.

We make use of the loss-cone analysis. We first define the loss cone fraction, F_q , which is the fraction of systems for which $q \leq a_1$. The condition of $q = a_1$ defines the critical eccentricity e_c , where the TBH would destabilize, namely

$$a_2 \cdot (1 - e_c) = a_1 \quad (2)$$

which corresponds to $e_c = 1 - a_1/a_2$.

$$F_q = \int_{e_c}^1 2ede = \frac{2a_1}{a_2}. \quad (3)$$

We note that $F_q \ll 1$. When a TBH is in the loss cone m_3 enters the inner binary within a outer orbital period

timescale, P_2 and the triple destabilize it is than lost from the ensemble of TBHs, and may contribute to the production of GW sources as we discuss below. Systems which orbits are close to the loss cone regime could potentially be perturbed into it and replenish the loss cone after the next flyby interaction. In order to calculate what is the fraction of such systems out of the entire ensemble we calculate the smear cone, the average size of phase space an outer binary can occupy after an impulsive interaction with flyby star. The smear cone, defined by $\theta = \langle \Delta v \rangle / v_k$, where v_k is the Keplerian velocity of the outer binary at the average separation, $\langle r \rangle = a_2 (1 + 1/2e^2)$. Because $F_q \ll 1$ we approximate $e \rightarrow 1$, namely $v_k = (GM/3a_2)^{1/2}$, where G is Newton's constant. The change in velocity $\Delta v \approx 3Ga_2m_p/v_{\text{env}}b^2$ (Hills 1981; Michaely & Perets 2019) where m_p is the mass of the flyby perturber. Following (Michaely & Perets 2019)... the size of the smear cone is

$$F_s = \frac{\pi\theta^2}{4\pi} = \frac{27}{4} \left(\frac{m_p}{M}\right)^2 \left(\frac{GM}{a_2v_{\text{enc}}^2}\right) \left(\frac{a_2}{b}\right)^4. \quad (4)$$

The ratio of the smear cone to loss cone is the fraction of the loss cone filled after a single flyby:

$$\frac{F_s}{F_q} = \frac{27}{8} \left(\frac{m_p}{M}\right)^2 \left(\frac{GM}{a_2v_{\text{enc}}^2}\right) \left(\frac{a_2}{b}\right)^4 \left(\frac{a_2}{a_1}\right). \quad (5)$$

In the case where the loss cone is continuously fully replenished, $F_q = F_s$, the timescale for the loss-cone replenishment becomes comparable to the timescale for the loss-cone depletion, i.e. the outer orbit orbital period, P_2 . Therefore the rate of depletion which is a function of the size of the loss cone is

$$\dot{L}_{\text{Full}} = \frac{F_q}{P_2} \propto a_2^{-5/2} a_1, \quad (6)$$

which is independent of the local stellar density, n_* and scales linearly with the inner binary SMA, a_1 . Therefore the depletion rate decreases with increasing outer SMA in the full loss cone regime.

On the other hand, for the case where $F_s < F_q$, namely for tighter outer binaries, which are less susceptible for change due to random flyby interaction (4), the loss cone is not completely full at all times, and one needs to consider the so called empty loss cone regime. In this case the depletion rate depends on the rate of systems being kicked into the loss cone. Specifically, $f = n_*\sigma v_{\text{enc}}$ where $\sigma = \pi b^2$ is the geometric cross-section of the random flyby interaction. In this case the typical timescale for the depletion is the timescale for entering the loss cone, namely $T_{\text{empty}} = 1/f$. As we showed previously, f can be written as (Michaely & Perets 2016, 2019)

$$f = n_*\pi\sqrt{\frac{27}{8} \left(\frac{m_p}{M}\right)^2 \frac{GMa_2^4}{a_1}}. \quad (7)$$

The critical SMA for which the two timescales are equal the depletion rate is equal to the rate of systems entering the loss cone (Michaely & Perets 2019) is given by

$$a_{\text{crit}} = \left(\frac{2}{27\pi^4} \frac{M}{m_p^2} \frac{a_1}{n_*}\right)^{1/7}. \quad (8)$$

Using a_{crit} we can calculate the fraction of systems that enter the loss cone for both regimes: $a < a_{\text{crit}}$ the empty loss cone; $a > a_{\text{crit}}$ the full loss cone.

The loss cone, F_q represents the fraction of systems that are lost from the ensemble after the relevant timescale, therefore $(1 - F_q)$ is the surviving fraction. For the empty loss cone regime this timescale is $T_{\text{empty}} = 1/f$ while for the full loss cone the timescale is P_2 . We can write the fraction of systems that enter the loss cone as function of time, t as

$$L(a_1, a_2, n_*)_{\text{empty}} = 1 - (1 - F_q(a_1, a_2))^{t/f}. \quad (9)$$

At the limit where $F_q t / T_{\text{empty}} \ll 1$ we can expand this equation to the leading order and get

$$L(a_1, a_2, n_*)_{\text{empty}} = F_q t f. \quad (10)$$

Note that the fraction of systems lost in the empty loss cone regime is proportional to F_q , namely

$$L_{\text{empty}} \propto F_q \propto a_2^{-1} a_1. \quad (11)$$

Specifically, the fraction grows with SMA for $a_2 < a_{\text{crit}}$, unlike the full loss cone regime. This means that the loss-rate peaks for TBHs with SMA of a_{crit} . For the full loss cone we follow the same treatment with

$$L(a_1, a_2, n_*)_{\text{full}} = 1 - (1 - F_q(a_1, a_2))^{t/P_2}, \quad (12)$$

and after the expansion we get

$$L(a_1, a_2, n_*)_{\text{full}} = F_q t / P_2. \quad (13)$$

Our treatment so far neglected the ionization process for wide systems in collisional environments. Taking the ionization into account by using the half-life time treatment from (Bahcall et al. 1985), where the half life time is defined to be

$$t_{1/2} = 0.00233 \frac{v_{\text{enc}}}{Gm_p n_* a_2} \quad (14)$$

we get for the empty loss cone

$$L(a_1, a_2, n_*)_{\text{empty}} = \tau F_q f (1 - e^{-t/\tau}) = \quad (15)$$

$$\tau \frac{2a_1}{a_2} n_* \pi \sqrt{\frac{27}{8} \left(\frac{m_p}{M}\right)^2 \frac{GMa_2^4}{a_1}} (1 - e^{-t/\tau}).$$

where $\tau = t_{1/2} / \ln 2$. For the full loss cone we get

$$L(a_1, a_2, n_*)_{\text{full}} = \tau \frac{F_q}{P_2} (1 - e^{-t/\tau}) = \quad (16)$$

$$\tau \frac{2a_1}{a_2} \left(\frac{GM}{4\pi^2 a_2^3}\right)^{1/2} (1 - e^{-t/\tau}). \quad (17)$$

We emphasize the fact that in both regimes the loss-cone fraction is proportional to the inner SMA a_1 . We can identify the loss-fraction to be the probability for a TBH to become unstable due to flyby interactions. Figure 2 shows a representative case for the probability of becoming unstable as a function of the outer SMA for some specific time during the evolution and for a specific given field environment.

Equipped with these equations we turn to calculate the fraction of GW-mergers that occur following the strong encounter between the outer third companion and the inner binary (i.e. the now unstable triple) catalyzed by the flyby perturbations.

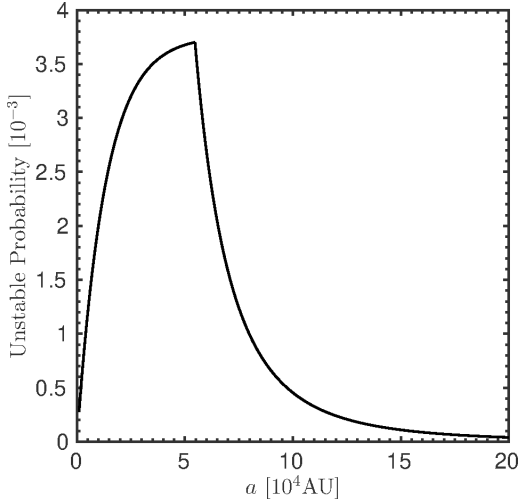


Figure 2. The probability of becoming unstable, namely the outer pericenter distance $q_2 = a_2(1 - e_2) \leq a_1$, due to flyby interaction. The plot is calculated for the following parameters: $t = 10\text{Gyr}$, $n_* = 0.1\text{pc}^{-3}$, $v_{\text{enc}} = 50\text{kms}^{-1}$. The highest probability is for a_{crit} . The full loss cone regime is for $a > a_{\text{crit}}$ and the empty loss cone regime is for $a < a_{\text{crit}}$.

3 UNSTABLE TRIPLES

In this section we describe the dynamics of unstable triples. We follow closely the treatment done by (Samsing et al. 2014, 2018a) in the context of binary-single encounters. It is well known that triple systems are not believed to be integrable and therefore we cannot predict the end result of any specific triple system. However, in a statistical manner we can predict the end state of binary-single encounter (Stone & Leigh 2019; Samsing et al. 2014; Heggie 1975).

Binary-single encounters are an important astrophysical source of unstable triples. The physics of binary-single encounters were studied mainly in dense stellar environment such as globular clusters or galactic nuclei. A close binary-single interaction is considered when the single star passes within the binary SMA, or specifically within the sphere of influence of the binary. In this situation the gravitational interaction between every pair of masses is comparable in strength and the outcome is chaotic. For such close interactions two outcomes are possible. The first, direct interaction (DI) where only one gravitational interaction takes place and the result is a tighter binary and an escaper. Note the binary could be either the same as in the initial condition, this case is called a *flyby*, or different and this case is called an *exchange*. The second, intermediate state (IMS), where the system goes through many (of the order of $\langle N_{\text{IMS}} \rangle = 20$, for our case (Samsing & Ramirez-Ruiz 2017)) binary-single encounters, where each time the orbital characteristics (SMA and eccentricity) are drawn from the available phase space volume set by the system angular momentum and energy budget. Keep in mind that when the binary orbital properties are set, conservation of angular momentum and energy set the trajectory of the bound third star until the next binary-single scatter. The end-state of the multiple binary-single scattering is a tight binary and an escaper.

From the GW perspective a merger can occur either promptly between scattering events during the IMS, or later,

after an end-state is reached, when one of the BHs escapes, leaving behind a more compact, likely eccentric binary. The remnant binary would eventually inspiral and merge through GW-emission on a typically much longer timescale than the dynamical time. A fraction of latter mergers occur in less than a Hubble time and these would contribute to the rate of detectable GW sources; we term this GW-sources channel the delayed-merger channel. In the following we calculate the rate of mergers and eccentricity distribution of the merged systems in both cases.

3.1 Binary-single encounters and the production of prompt GW-mergers

In this subsection we describe the mathematical modeling of the IMS. In the following we consider only equal masses BH with $10M_{\odot}$ each. The initial binary is circular with SMA, a_1 , and the third BH interacts with the binary via consecutive binary-single encounters. In each encounter the probability for forming a temporary binary with any two out of the three BHs is uniform. The eccentricity, e_{IMS} is drawn from thermal distribution, namely $f(e)de = 2ede$. The SMA is determined by the energy budget which is approximated by equation 12 in (Samsing et al. 2018a)

$$\frac{m_1 m_2}{2a_1} = \frac{m_i m_j}{2a_{\text{IMS}}} + \frac{m_{ij} m_k}{2a_{\text{bs}}} \quad (18)$$

where a_{IMS} is the SMA of the temporary binary and a_{bs} is the temporary SMA of the outer binary. Where $\{i, j, k\}$ are the randomized indexes after the interaction and $m_{ij} = m_i + m_j$ is the mass of the temporary binary. From eq. (18) we can express the SMA of the third bound BH

$$a_{\text{bs}} = a_1 \left(\frac{m_{ij} m_k}{m_1 m_2} \right) \left(\frac{a'}{a' - 1} \right) \quad (19)$$

where

$$a' \equiv \frac{a_{\text{IMS}}}{a_c} \text{ and } a_c \equiv a_1 \frac{m_i m_j}{m_1 m_2}. \quad (20)$$

We note that in our equal mass case $a_c = a_1$ and therefore a' is just a_{IMS}/a_1 .

In order to estimate the available phase space for the IMS we estimate the upper (lower) bound a'_{U} (a'_{L}) of a' . The lower bound of a' is trivial with

$$a'_{\text{L}} \approx 1, \quad (21)$$

the upper bound should separate between when the resonant triple can no longer be described as an IMS (a binary and a bound single), this occurs when $a_{\text{bs}} \approx a_{\text{IMS}}$. Samsing et al. (2018a) finds that one way of estimating a'_{U} is by comparing the tidal force, F_{tid} exerted by the third BH with the binary gravitational binding force, F_{bin} . In the high eccentricity limit we find

$$F_{\text{tid}} \approx \frac{1}{2} \frac{G m_{ij} m_k}{a_{\text{bs}}^2} \frac{a_{\text{IMS}}}{a_{\text{bs}}} \quad (22)$$

$$F_{\text{bin}} \approx \frac{1}{4} \frac{G m_i m_j}{a_{\text{IMS}}^2}. \quad (23)$$

We set a'_{U} in the case that

$$\frac{F_{\text{tid}}}{F_{\text{bin}}} = 0.5 \quad (24)$$

which translates to

$$a'_U = 1 + \left(\frac{1}{2} \frac{m_k}{\mu_{ij}} \right)^{2/3} \quad (25)$$

where $\mu_{ij} \equiv m_i m_j / (m_i + m_j)$ is the reduced mass of the IMS binary.

The values of a' are distributed uniformly between a'_L and a'_U and the eccentricity distribution is thermal (Heggie 1975; Hut & Tremaine 1985; Rodriguez et al. 2018).

Next we can calculate the orbital timescale for the third companion, t_{iso} , to come back for the next binary-single encounter. During the tie in-between scatter events the temporary binary can potentially merge via GW emission if its merger timescale, t_{merger} is shorter than t_{iso} .

The orbital period is simply the Keplerian orbital period with a_{bs} ; combining it with eq. (19) and eq. (20) we get:

$$t_{\text{iso}} = 2\pi \frac{a_1^{3/2}}{\sqrt{GM}} \left(\frac{m_{ij} m_k}{m_1 m_2} \right)^{3/2} \left(\frac{a'}{a' - 1} \right)^{3/2}. \quad (26)$$

The merger timescale, for eccentric binaries, is given by (Peters 1964)

$$t_{\text{merger}} \approx \frac{768}{425} T_c(a_{\text{IMS}}) (1 - e_{\text{IMS}}^2)^{7/2} \quad (27)$$

where $T_c = a_{\text{IMS}}^4 / \beta$ is the merger timescale for a circular orbit and $\beta = 64 G^3 m_i m_j (m_i + m_j) / (5c^2)$ where c is the speed of light.

3.1.1 Calculating the merger fraction

In order to find the fraction of systems that merge during the IMS as a function of the initial SMA, a_1 , we **perform a numerical calculation. In order to save computer time we do not make a direct N-body simulation. We sample, in a Monte-Carlo approach, the IMSs orbital distributions from (Samsing et al. 2014; Samsing & Ramirez-Ruiz 2017) and check whether or not they lead to a merger. We use MATLAB to sample 20 values of a_1 equally spaced in log from (10^{-2} AU, 10^2 AU). For each value of a_1 we simulate $N_{\text{tot}} = 10^5$ scattering experiments where for each scattering experiment there is $N_{\text{IMS}} = 20$ times where a temporary binary is created bound to a third BH on a Keplerian orbit. For each iteration of the IMS we randomly choose the binary orbital properties, a_{IMS} , which are drawn from a uniform distribution in the range (a'_L, a'_U) see equations (21) and (25); and the eccentricity, e_{ecc} is drawn from a thermal distribution. Next, we calculate t_{iso} from eq. (26) and compare it to t_{merger} from eq. (27). If $t_{\text{merger}} < t_{\text{iso}}$ we count it as an IMS merger and check whether it is an eccentric merger in the LIGO band, see subsection 3.1.2. If $t_{\text{merger}} > t_{\text{iso}}$ we randomize the binary and single again until we reach N_{IMS} times. Additionally we record all t_{iso} in order to calculate the merger time since the beginning of the scattering experiment. In the case where no merger occurs during the resonant phase we record the final end state, to eventually obtain the distribution of the orbital parameters from such cases (see subsection 3.2). $f_{\text{merger}}(a_1)$ is then just the number of mergers divided by the total number of systems considered, N_{tot} . The results presented in Figure 3. We find a power law relation between f_{merger} and a_1 , the exact fitted**

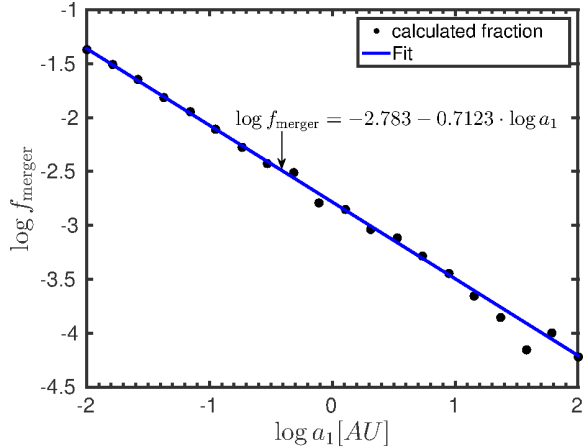


Figure 3. The fraction of systems that merged, f_{merger} during the resonant phase as a function of the initial SMA, a_1 . For every a_1 we simulated 10^5 binary-single scattering experiments; for each experiment we use $N_{\text{IMS}} = 20$ scattering events which we randomize the temporary binary orbital elements (see text) and check if this temporary IMS leads to a merger. Black dots, the calculated fraction from our numerical experiment. Blue solid line, the best fit to a power law.

function is

$$f_{\text{merger}}(a_1) = 0.00165 \times a_1^{-0.7123}. \quad (28)$$

We note that the fraction scales with the inner SMA with a power which is smaller than unity $f_{\text{merger}} \propto a_1^{-0.7123}$.

3.1.2 Calculating the fraction of eccentric mergers

In order to find $f_{\text{eccentric}}(a_1)$ we simulate the evolution of each binary we flagged as an IMS merger. We use the well known equations of motion of the SMA and eccentricity from (Peters 1964)

$$\frac{da}{dt} = -\frac{64}{5} \frac{G^3 m_1 m_2 (m_1 + m_2)}{c^5 a^3 (1 - e^2)^{7/2}} \left(1 + \frac{73}{24} e^2 + \frac{37}{96} e^4 \right) \quad (29)$$

$$\frac{de}{dt} = -e \frac{304}{15} \frac{G^3 m_1 m_2 (m_1 + m_2)}{c^5 a^4 (1 - e^2)^{5/2}} \left(1 + \frac{121}{304} e^2 \right). \quad (30)$$

Additionally we calculate the approximate gravitational peak frequency following (Wen 2003)

$$f_{\text{peak}}(a_{\text{IMS}}, e_{\text{IMS}}) = \frac{1}{\pi} \sqrt{\frac{G m_{ij}}{a_{\text{IMS}}^3}} \frac{(1 + e_{\text{IMS}})^{1.1954}}{(1 - e_{\text{IMS}}^2)^{1.5}}. \quad (31)$$

We consider a binary merger to be an eccentric merger if the eccentricity, e_{IMS} is greater than 0.1 when the GW peak frequency is $f_{\text{peak}} = 10$ Hz (e.g. Rodriguez et al. 2018). In Figure 4 we present our calculated eccentric merger fraction as a function of the initial SMA, a_1 . The relation between the eccentric fraction and the initial SMA is well described by a power law

$$f_{\text{eccentric}}(a_1) = 0.0006 \times a_1^{-0.942}. \quad (32)$$

In Figure 5 we present the eccentricity distribution at 10 Hz for the entire sample weighted by the inner SMA distribution. We report that $\sim 78\%$ of all mergers in the IMSs are eccentric in the aLIGO band.

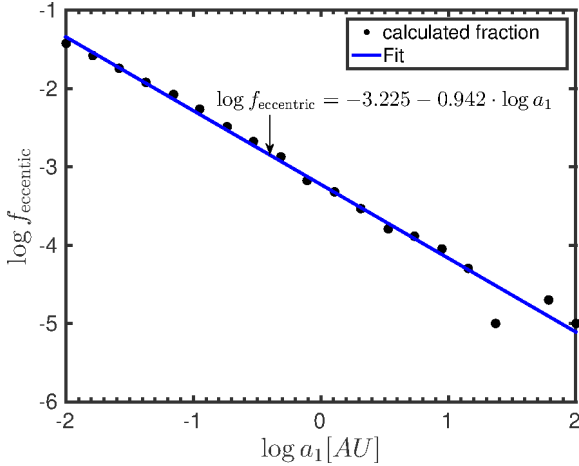


Figure 4. The fraction of eccentric mergers, $f_{\text{eccentric}}$ during the resonant phase as a function of the initial SMA, a_1 . For the same setup as in Figure 3. Black dots, the calculated fraction from our numerical experiment. Blue solid line, the best fit to a power law.

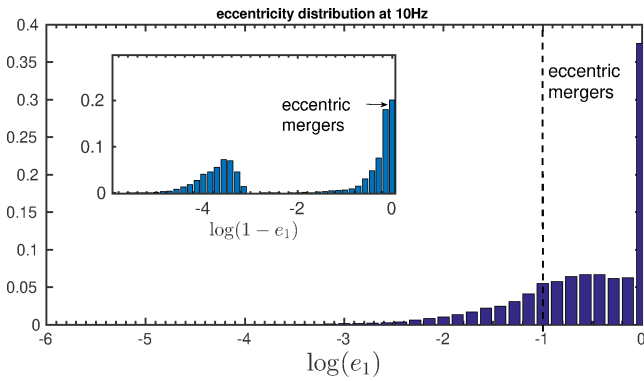


Figure 5. The eccentricity distribution at 10Hz GW frequency of our entire sample. The main plot show the distribution of $\log e$, hence all values greater than -1 are eccentric mergers, $\sim 78\%$. This distribution is weighed with the distribution of the initial SMA, a_1 . The inset is the same distribution but presented in $\log(1 - e_1)$, namely focuses on the most eccentric part of the distribution we see the most probable e value correspond to $\log(1 - e_1) \approx -3.5$.

3.2 The post encounter states and the production of delayed-mergers

In the following we study the the production of delayed mergers in cases where no prompt merger occurs during the resonant encounter, and a remnant compact binary is formed with $a_{\text{delay}} < a_1$ (while the third BH is ejected from the system). It was shown in (Stone & Leigh 2019) that the energy distribution of the remnant binary scales like

$$E_{\text{delay}} \propto |E_1|^{-4} \quad (33)$$

where E_{delay} is the energy of the remnant binary and $E_1 = -Gm_1m_2/(2a_1)$ is the initial binary energy.

Additionally, the eccentricity of the remnant binary, e_{delay} , is drawn from thermal distribution (Stone & Leigh 2019).

For every system that did not promptly merge during the IMS we follow the GW-inspiral evolution of the remnant

binary and calculate the merger time by using eq. (27), and the eccentricity at $f_{\text{peak}} = 10\text{Hz}$ by following the same treatment as described in (3.1.2) for the prompt mergers, where the only difference is such binaries are followed up to a Hubble time, as their evolution is not restricted by the next encounter (i.e. at the isolation time). The left panel of Figure 6 shows the fraction of systems that merge within a Hubble time, and the eccentricity distribution for our sample, weighted by the distribution of the inner SMA, is presented in the right panel. We note that the eccentricity distribution is very similar to (Rodriguez et al. 2018; Samsing et al. 2018b), besides the somewhat lower fraction of eccentric mergers, as these mergers do not include the prompt mergers discussed before. The combined distribution of both the prompt and delayed mergers is comparable with those found by (Rodriguez et al. 2018), as might be expected given that the final distribution in both cases is generally determined by the outcomes of binary-single encounters.

We found a numerical Gaussian fit to the merger fraction of the delayed mergers

$$\log f_{\text{delay}} = -3.237 \times e^{-\left(\frac{\log a_1 - 2.212}{1.964}\right)^2}, \quad (34)$$

and find that the total fraction of eccentric delayed mergers is $f_{\text{delay, ecc}} \approx 1\%$.

We note that the majority of the prompt mergers are eccentric because the merger time is limited to the isolation time $t_{\text{iso}} \ll t_{\text{Hubble}}$, and only the most initially eccentric binaries, having small peri-centers, could merge on such short timescales. In contrast, we find a smaller fraction of eccentric delayed mergers because the merger time is instead limited by t_{Hubble} , allowing for binaries that merge on these longer timescales to also circularize by the time they reach the aLIGO band.

We emphasize that isolated binaries with SMA smaller than 0.1AU will merge within a Hubble time, therefore we expect the fitted function from equation (34) to saturate at the lower end of a_1 near unity. The merger rate we calculate for these binaries is therefore effectively included in the isolated binary channels discussed by others (Belczynski et al. 2016, 2008; Dominik et al. 2012, and others). Nevertheless, the IMS evolution could give rise to higher initial eccentricity of such binaries and thereby (on average) shorter merger time and potentially higher detected eccentricities, even if not affecting the total merger rate. Although this is generally the case, in terms of longer delay times, the relatively low fraction of eccentric mergers coming from these (small initial SMA) mergers indicates that these mergers are effectively indistinguishable from the isolated binary case at least in the aLIGO band. One should note that they may still present significantly higher eccentricities at earlier stages, potentially observable by future space-based GW-detectors. The latter aspects, however, are beyond the scope of the current paper.

4 VOLUMETRIC RATES OF GW-SOURCES FROM THE TBH CHANNEL

In this section we calculate the volumetric rate of GW mergers from TBHs in both the prompt and delayed mergers channels. We make use of the equations (15) and (16) to calculate the fraction of TBHs that become unstable due

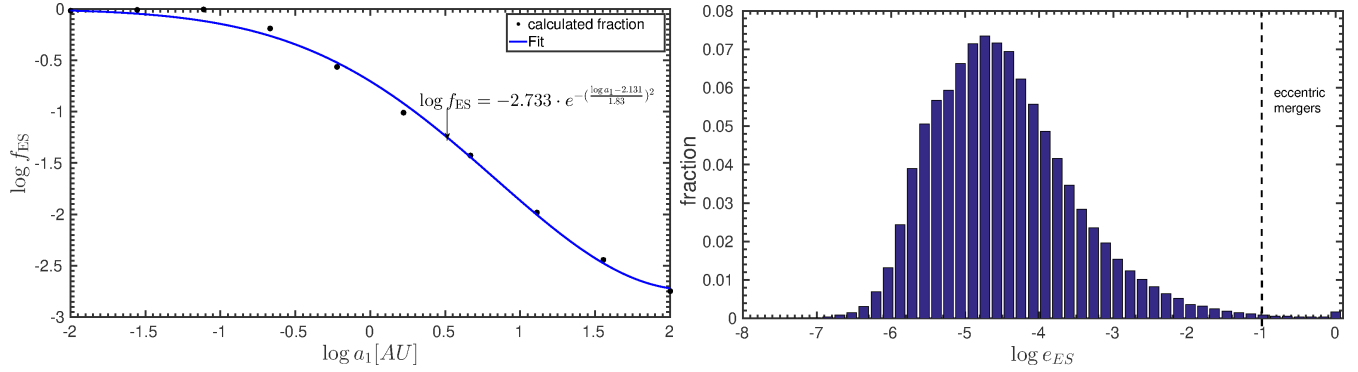


Figure 6. Left plot: The fraction of delayed mergers, f_{delay} as a function of the initial SMA, a_1 out of 10^4 binary-single experiments. A merger is flagged when the merger timescale is less than the Hubble time, t_{Hubble} . Black dots, the calculated fraction from our numerical experiment. Blue solid line, the best fit to a Gaussian with the variable, $\log a_1$. Right plot: The eccentricity distribution at 10Hz for all delay mergers, weighted with the initial SMA, a_1 distribution. The plot is similar to (Rodríguez et al. 2016; Samsing & Ramirez-Ruiz 2017). Only $\sim 0.3\%$ of the entire population is eccentric at $\sim 10\text{Hz}$

to flybys, and then combine them with the merger fractions described above, f_{merger} and f_{ecc} (from equations (28) and (32)). Since the different properties of spiral and elliptical galaxies affect the rates (through the different stellar number density and velocity dispersions in the different types of galaxies), we calculate the merger rate for both typical spiral and elliptical galaxies. For the spiral galaxy case we model a Milky Way (MW)–like galaxy stellar density similar to that considered in (Michaely & Perets 2016). Let $dN(r) = n_*(r) \cdot 2\pi \cdot r \cdot h \cdot dr$ be the the number of stars in a region dr (and scale height h), located at distance r from the center of the Galaxy. Additionally, we model the Galactic stellar density in the Galactic disk as follows

$$n_*(r) = n_0 e^{-(r-r_\odot)/R_l} \quad (35)$$

, where $n_0 = 0.1\text{pc}^{-3}$ is the stellar density near our Sun, $R_l = 2.6\text{kpc}$ (Jurić et al. 2008) is the galactic length scale and $r_\odot = 8\text{kpc}$ is the distance of the Sun from the galactic center. The mass of the perturber is taken to be $0.6M_\odot$ which is the average mass of a star in the galaxy. The velocity dispersion is set to the velocity dispersion of the flat rotation curve of the galaxy, namely $\sigma = 50\text{kms}^{-1}$.

For elliptical galaxies we take the density profile from (Hernquist 1990) and translate it to stellar density given an average stellar mass of $0.6M_\odot$.

$$\tilde{n}_*(r) = \frac{M_{\text{galaxy}}}{2\pi r} \frac{r_*}{(r + r_*)^3} \quad (36)$$

where $r_* = 1\text{kpc}$ is the scale length of the galaxy, $M_{\text{galaxy}} = 10^{11}M_\odot$ is the total stellar (and not total) mass of the galaxy. The velocity dispersion for a typical elliptical galaxy we consider is $\sigma = 160\text{kms}^{-1}$. Figure 7 shows the stellar density profiles of the two prototypes of galaxies.

Next, we estimate the fraction of TBHs out of the entire stellar population, f_{TBH} . The fraction of BHs out of the entire stellar population is $f_{\text{primary}} \approx 10^{-3}$ (Kroupa 2001). We assume all stars with masses greater than $20M_\odot$ turn into BHs without any natal-kicks (Belczynski et al. 2016; Mandel 2016, and others) and the triple fraction of all BHs progenitors is $f_{\text{triple}} = 0.25$ (Sana et al. 2014). For the mass ratio distribution in the inner binary, Q_{inner} we consider a uniform distribution $Q_{\text{inner}} \in (0.3, 1)$ (Moe & Di Stefano 2016), this

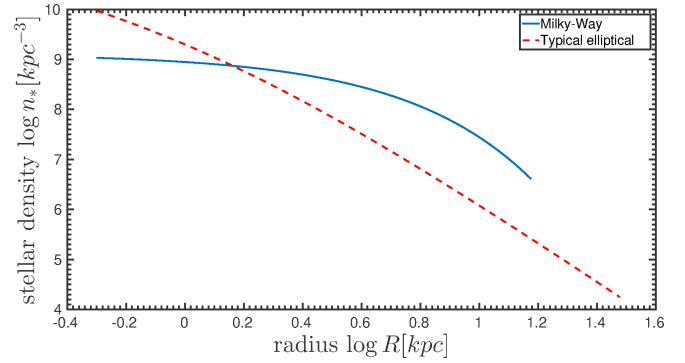


Figure 7. Number stellar density as a function of distance. The blue solid line represents the Milky-Way galaxy. The red dashed line represents a typical elliptical galaxy.

translates to a fraction of $f_{\text{secondary}} \approx 0.53$ of the inner binary companions to also form BHs. Additionally, we can compute the fraction of the inner binaries (accounting for their total main-sequence masses) to have a third BH progenitor companion, in this case we use a different mass ratio distribution $Q_{\text{outer}} \propto M_{\text{binary}}^{-2}$ (Moe & Di Stefano 2016), as to apply for wide separation systems, and consider the range $Q_{\text{outer}} \in (0.3, 1)$. M_{binary} is the total mass of the inner binary. This translates to the fraction of the tertiaries forming BHs of $f_{\text{traiery}} \approx 0.76$. Hence the total fraction of TBHs from the stellar population is

$$f_{\text{TBH}} = f_{\text{primary}} \times f_{\text{secondary}} \times f_{\text{tertiary}} \times f_{\text{triple}} \approx 1 \times 10^{-4}. \quad (37)$$

The SMA distribution f_{a_1} and f_{a_2} is taken to be a log-uniform, where the inner binary SMA ranges between $a_1 \in (0.1\text{AU}, 100\text{AU})$ while $a_2 \in (10^3\text{AU}, 10^5\text{AU})$. Following (Michaely & Perets 2019; Perets & Kouwenhoven 2012; Igoshev & Perets 2019) we take the overall fraction of triple systems that are wider than 10^3AU to be $f_{\text{wide}} = 0.2$.

4.1 Volumetric prompt-merger rates

In the following we calculate the volumetric delayed-merger rate and the volumetric eccentric delayed-merger rate.

Spiral galaxies

For a MW-like galaxy the rate of BH prompt GW-mergers from perturbed wide TBH in the field is just

$$\Gamma_{\text{MW}} = \int_{0.5\text{kpc}}^{15\text{kpc}} \int_{10^3\text{AU}}^{10^5\text{AU}} \int_{10^{-1}\text{AU}}^{10^2\text{AU}} \frac{L_{\text{merger}}(a_1, a_2, n_*)}{10\text{Gyr}} da_1 da_2 dN(r) \quad (38)$$

$$\approx 0.017\text{Myr}^{-1}$$

where $L_{\text{merger}} \equiv L(a_1, a_2, n_*) f_{a_1} f_{a_2} f_{\text{TBH}} f(a_1)_{\text{merger}}$. In order to translate this rate to the volumetric merger rate in spiral galaxies R_{spiral} , we follow (Belczynski et al. 2016) and calculate the rate $R_{\text{spiral}} = 10^3 n_{\text{spiral}} \times \Gamma_{\text{MW}}$, to get

$$R_{\text{spiral}} \approx 0.2 \times F_{\text{model}} \text{Gpc}^{-3} \text{yr}^{-1}. \quad (39)$$

Where $n_{\text{spiral}} = 0.0116\text{Mpc}^{-3}$ is the local density of MW-like galaxies (Kopparapu et al. 2008) and we define

$$F_{\text{model}} \equiv \left(\frac{f_{\text{primary}}}{10^{-3}} \right) \left(\frac{f_{\text{secondary}}}{0.53} \right) \left(\frac{f_{\text{teritary}}}{0.76} \right) \left(\frac{f_{\text{wide}}}{0.2} \right) \left(\frac{f_{\text{triple}}}{0.25} \right) \quad (40)$$

to be the how the results depend on our model assumption. Moreover, we can calculate the eccentric merger rate from this channel simply by substituting f_{merger} with f_{ecc} from equation (5), to find

$$\Gamma_{\text{MW,ecc}} = \int_{0.5\text{kpc}}^{15\text{kpc}} \int_{10^3\text{AU}}^{10^5\text{AU}} \int_{10^{-1}\text{AU}}^{10^2\text{AU}} \frac{L_{\text{ecc}}}{10\text{Gyr}} da_1 da_2 dN(r) \quad (41)$$

$$\approx 0.01\text{Myr}^{-1}.$$

where $L_{\text{ecc}} \equiv L_{\text{merger}}(a_1, a_2, n_*) f_{a_1} f_{a_2} f_{\text{TBH}} f(a_1)_{\text{eccentric}}$. Hence,

$$R_{\text{spiral,ecc}} \approx 0.12 \times F_{\text{model}} \text{Gpc}^{-3} \text{yr}^{-1}, \quad (42)$$

and the fraction of eccentric mergers from this channel is consistent with $\sim 78\%$.

Elliptical galaxies

Following a similar procedure we now calculate the prompt-merger rate from elliptical galaxies. Taking Eq. (36)

$$\Gamma_{\text{elliptical}} = \int_{0.5\text{kpc}}^{30\text{kpc}} \int_{10^3\text{AU}}^{10^5\text{AU}} \int_{10^{-1}\text{AU}}^{10^2\text{AU}} \frac{L_{\text{merger}}(a_1, a_2, \tilde{n}_*)}{10\text{Gyr}} da_1 da_2 dN(r) \quad (43)$$

$$\approx 0.03\text{Myr}^{-1}.$$

Next we input the number density of elliptical galaxies in the local universe $n_{\text{elliptical}} \approx 0.1\text{Mpc}^{-3}$ (Samsing et al. 2014) and get

$$R_{\text{elliptical}} = 3.2 \times F_{\text{model}} \text{Gpc}^{-3} \text{yr}^{-1}. \quad (44)$$

and for the eccentric mergers we get

$$R_{\text{elliptical,ecc}} = 1.2 \times F_{\text{model}} \text{Gpc}^{-3} \text{yr}^{-1}. \quad (45)$$

Adding the contributions from both spiral and elliptical galaxies we get a total volumetric prompt-merger rate to be

$$R_{\text{resonant}} = R_{\text{spiral}} + R_{\text{elliptical}} \approx 3.4 \times F_{\text{model}} \text{Gpc}^{-3} \text{yr}^{-1}. \quad (46)$$

and the volumetric eccentric prompt-mergers

$$R_{\text{resonant,ecc}} = R_{\text{spiral,ecc}} + R_{\text{elliptical,ecc}} \approx 1.2 \times F_{\text{model}} \text{Gpc}^{-3} \text{yr}^{-1} \quad (47)$$

4.2 Volumetric delayed merger rates

In the following we calculate the volumetric delayed-merger rate and the volumetric eccentric delayed-merger rate. Following the same procedure described in subsection 3.2 we calculate the merger rate by substituting f_{merger} with f_{delay} from equation (34). As done in the previous section, we calculate the merger rate of systems with $a_1 \in (10^{-1}\text{AU}, 10^2\text{AU})$ for both types of galaxies.

For spiral galaxies we find

$$\Gamma_{\text{spiral,delay}} \approx 0.9\text{Myr}^{-1} \quad (48)$$

which leads to

$$R_{\text{spiral,delay}} \approx 9.2 \times F_{\text{model}} \text{Gpc}^{-3} \text{yr}^{-1}. \quad (49)$$

For elliptical galaxies we find

$$\Gamma_{\text{elliptical,delay}} \approx 1.5\text{Myr}^{-1} \quad (50)$$

which translates to

$$R_{\text{elliptical,delay}} \approx 150 \times F_{\text{model}} \text{Gpc}^{-3} \text{yr}^{-1}. \quad (51)$$

In total we compute a volumetric rate of

$$R_{\text{delay}} = R_{\text{spiral}} + R_{\text{elliptical}} \approx 160 \times F_{\text{model}} \text{Gpc}^{-3} \text{yr}^{-1}. \quad (52)$$

Unlike the prompt-mergers only $\sim 0.3\%$ of delayed-mergers end up as eccentric at 10Hz. Therefore we expect only $\sim 0.5 \times F_{\text{model}} \text{Gpc}^{-3} \text{yr}^{-1}$ eccentric volumetric rate mergers from this channel.

5 DISCUSSION

5.1 Model assumptions

The progenitor model for BBH GW-merger presented makes use and is based on several assumptions, in the following we address each them.

Natal kicks. We cannot emphasize this point enough. This is the *most* critical assumption we make is that the BHs discussed here, receive no natal kick at birth. The importance of this assumption, as we discussed in more depth in (Michaely & Perets 2019), is that ultra-wide binaries/triples are highly susceptible to disruption by such kicks. The binding energy of the outer binary in the triple are very small, and natal-kicks of comparable velocity to the typical orbital velocity of the outer orbit or higher would disrupt the triple, significantly decreasing the number of potential TBH progenitors as discussed in (Silsbee & Tremaine 2017).

Currently, BH natal kicks are poorly constrained (Repetto et al. 2012, 2017). However, there is some evidence that BH are formed following failed supernova (SN)

(Ertl et al. 2015; Adams et al. 2017). In the failed SN scenario large amount of fallback is accreted on the newly formed compact object and suppresses any natal kicks, as the BH forms through direct collapse (Fryer et al. 1999). In fact, most if not all other theoretical models that can potentially reproduce the inferred high rates of BBH GW-mergers follow similar assumptions, and also assume no or low-velocity natal-kicks for BHs, or no/low natal kicks for higher mass BHs that form through direct collapse (e.g. Belczynski et al. 2016, 2008, 2007, where many of the dynamical models make use of the same assumptions). We generally follow the same approach.

Equal BH masses. Here we considered only TBHs composed of same-mass BH components. This simplistic assumption is made as a first step in developing this model. In the future we will expand the mathematical formalism to account for unequal masses. Nevertheless, we do not expect the rate to change dramatically (e.g. Samsing et al. 2018a), when unequal BHs are considered.

Nevertheless, we briefly discuss possible implications of our model in respect to the mass-function of the GW-mergers. The masses of the component of the inner binaries are likely to be correlated, as we discussed in the assumptions regarding the rate calculations in section 4 and generally be more similar to those expected from the isolated binaries channel, where short period binaries serve as GW-sources progenitors. The outer third component, might be expected to be randomly drawn from a regular mass-function, as it forms almost in isolation, given the large separation from the inner binary (although in case it was dynamically captured, e.g. Perets & Kouwenhoven (2012), it would have some preference to higher masses). Since typically the less massive component is ejected in binary-single encounters, the dynamics will systematically give rise to overall higher mass BHs to take part in mergers compared with the BH mass function of single, or even isolated binary BHs. A more detailed prediction, however, will require further study of the binary-single encounter dynamics of unequal mass TBHs.

Inner binary SMA boundaries. We set the lower boundary of the inner SMA to be $a_1 = 0.1\text{AU}$. The reason is that the merger time via GW emission of a circular binary with $m_1 = m_2 = 10M_\odot$ at $a_1 = 0.1\text{AU}$ is $t_{\text{merger}} \approx 10^{10}\text{yr}$. Hence, binaries with SMA smaller than 0.1AU may merge in isolation even without any perturbations, and thereby our model would not increase the GW-merger rates originating from such short-period binaries. Nevertheless, as we discussed above, such binaries which are part of TBHs such as those we discussed, might still evolve through the triple instability we present here, and in this case their merger characteristics will differ, in particular their eccentricities might be higher, they will have shorter DTD, and should not generally show a spin-orbit alignment.

For completeness we present in table 1 the volumetric merger rate accounting for binaries with initial SMA $a_1 = 10^{-2}\text{AU}$ in order to compare with our results.

Volumetric rate calculation. In order to calculate the volumetric rate we make the assumption that the galaxy densities, both spiral and elliptical are $n_{\text{spiral}} =$ and $n_{\text{elliptical}}$. Furthermore, we assume the MW is the prototype of spiral galaxies with velocity dispersion of 50kms^{-1} and total mass of $10^{11}M_\odot$ and the model we present in equa-

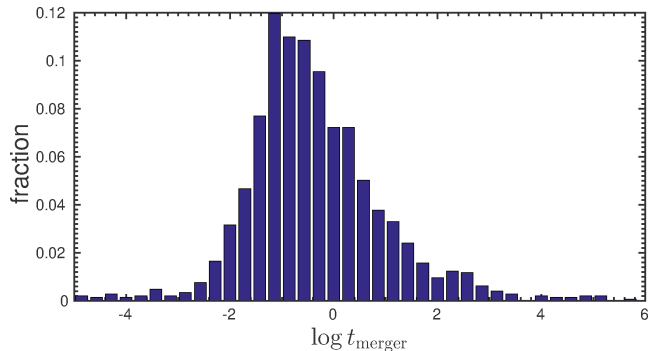


Figure 8. The distribution of merger times in the resonant phase. The merger time, $t_{\text{merger}} \lesssim P_2$ hence we regard of mergers from the resonant stage as prompt once the TBH becomes unstable

tion (36) is the prototype for elliptical with total mass of $10^{11}M_\odot$. This assumption may change the merger rate significantly for different galaxy prototypes. Specifically, for elliptical galaxies with total mass of $5 \times 10^{10}M_\odot$ the rate decreases by an order of magnitude. The sensitivity of our results by the specific model for a prototype galaxy motivates us to explore the issue in future research. Moreover, in Michaely & Perets (2019) we calculated the merger rate for wide binary systems solely for spiral galaxies. Following this work we argue that the rate of mergers from wide BBHs systems is governed from elliptical rather than spiral. We will explore this scenario elsewhere.

5.1.1 Delay time distribution (DTD)

Michaely & Perets (2019) showed that the DTD for wide binaries is uniform in time. A priori one would expect that the DTD for the TBH case might be more complicated due to the additional inspiral timescale during the resonant encounter or the later inspiral of the delayed mergers. In figure 8 we present the inspiral time for the prompt-mergers. We see that very short merger times $t_{\text{merger}} < 10^6\text{yr}$, which would hardly affect the overall uniform DTD for the initial production of the destabilized TBHs, and can be generally neglected in that context. The DTD for the prompt-GE channel is therefore expected to be generally uniform in time, similar to the ultra-wide binary channel discussed in (Michaely & Perets 2019).

The inspiral time of the delayed mergers is different (see figure 3). The distribution is dominated by a peak at $\sim 10^6\text{yr}$ approximately corresponding to the merger time of an initially circular binary with $a_1 = 0.01\text{AU}$ which is the most weighed value, given the assumed log uniform distribution of the SMAs. Considering a larger lower-bound $a_1 > 0.01\text{AU}$ the peak would shift and be centered around $t(a_1)_{\text{merger}}$, from equation (27) until $a_1 = 0.1\text{AU}$ which corresponds to a merger time of $\sim 10^{10}\text{yr}$ which is the upper cutoff. The shape to the right of the peak is effectively tracing the SMA distribution, f_a .

In this case the DTD would be slightly affected by the additional merger timescale for the shorter period binaries, and only somewhat change for the tail distribution of long merger times, giving rise to some modulation of the DTD, leading to a slightly decreasing DTD function.

We should also briefly note that at the early stages of

Table 1. The volumetric merger rates for the case where $a_1 \in (10^{-2}\text{AU}, 10^2\text{AU})$. Effectively these numbers include the isolated binary rates, hence they do not represent an *additional* contribution to the merger rates from the TBH channel.

	prompt mergers $F_{\text{model}}\text{Gpc}^{-3}\text{yr}^{-1}$	eccentric mergers $F_{\text{model}}\text{Gpc}^{-3}\text{yr}^{-1}$	delayed mergers $F_{\text{model}}\text{Gpc}^{-3}\text{yr}^{-1}$
spirals	~ 0.6	~ 0.5	~ 15
elliptical	~ 9.1	~ 8.6	~ 250

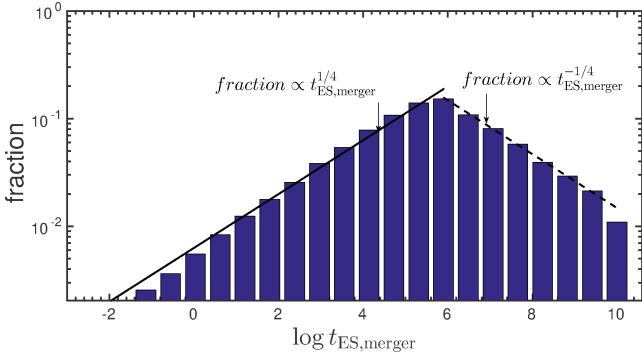


Figure 9. The inspiral time for all delayed mergers weighted by the distribution of the inner SMA, a_1 . Black solid line is to guide the eye with a slope that corresponds to $t_{\text{delay,merger}}^{1/4}$ and the black dashed line corresponds to $t_{\text{delay,merger}}^{-1/4}$.

galaxy formation, in particular in disk galaxies, the initial stellar densities and the number of BHs are initially low, compared to our basic model assumptions, accounting only for fully formed galaxies. However, this should hardly affect the observable GW-sources most of which would not originate from such early times.

5.1.2 Spin distribution

The dynamical process of multiple binary-single interactions effectively samples the phase space chaotically such that the end state inclination distribution is close to isotropic (Stone & Leigh 2019). It is likely that this similarly holds for the resonant phase as well, where multiple though smaller number of encounters occur, although such assumption needs to be better verified in future studies. Overall we expect to find, similar to dynamical mergers in dense environments, an isotropic distribution of the orbital inclination and therefore an isotropic spin-orbit alignment distribution. In that respect, the current findings of a preference for either an isotropic spin distribution or low spin magnitudes for the observed systems (Will 2014), are consistent with our suggested channel.

5.1.3 Eccentric mergers distributions

It was previously shown that eccentric mergers can originate from dynamical channels in dense cluster environments (e.g. Samsing & Ramirez-Ruiz 2017; Rodriguez et al. 2018), which predict a volumetric rate of eccentric mergers of $\sim 0.2 - 1\text{Gpc}^{-3}\text{yr}^{-1}$. As we show here, eccentric mergers can arise from the wide-TBH channel in the field. We find in equation (47) a volumetric rate of $\sim 5 \times F_{\text{model}}\text{Gpc}^{-3}\text{yr}^{-1}$

eccentric mergers from the prompt-merger channel, which dominate the contribution of eccentric mergers from this TBH scenario. Additionally, we present their distribution in the inset of figure 5 and expect a peak of the distribution with $\log(1 - e_1) \approx -3.5$. This extremely high eccentricities correspond to a unique signal in aLIGO/VIRGO.

Moreover, we find that, 0.3% of the delayed-mergers we studied are eccentric at 10Hz see figure 6. This correspond to a rate of $\sim 0.3 - 0.8 \times F_{\text{model}}\text{Gpc}^{-3}\text{yr}^{-1}$. Combining the prompt-merger and delayed-merger contributions we find an overall rate of eccentric mergers of

$$R_{\text{eccentric,TBH}} \approx 1 - 10 \times F_{\text{model}}\text{Gpc}^{-3}\text{yr}^{-1}. \quad (53)$$

6 SUMMARY

In this paper we extended our previous study of BBH GW-sources formation from ultra-wide binaries perturbed by random flyby encounters in the field, and studied ultra-wide triples. We calculate the merger rate and eccentric merger rate of BBH originating from this channel and find them to potentially be one of the main channels for BBH GW sources.

Wide TBH systems are gravitationally perturbed by random flybys of stars in the field, giving rise to a random walk of their outer-binary angular momentum. As a result a fraction of the TBH outer-binaries become highly eccentric and their pericenter is sufficiently decreased to give rise to a strong encounter between the outer TBH component and the inner binary, destabilizing the system and driving it into an effective binary-single resonant encounter similar to such encounters that drive dynamical formation channels of GW-sources in dense stellar clusters. Consequently the TBHs evolve through a sequence of many binary-single encounters, during which two of the BHs might merge in what we term a prompt-GE mergers. Alternatively, one of the BHs could be ejected, leaving behind a remnant, more compact BBH. In the later case, sufficiently compact remnant BBHs would inspiral and merger through GW emission, and contribute to the formation of detectable GW sources, in what we term the delayed-mergers channel. We find the total volumetric rate of systems that merge via GW emission from both channels to be

$$R_{\text{IMS,merger}} \approx 50 - 150 \times F_{\text{model}}\text{Gpc}^{-3}\text{yr}^{-1} \quad (54)$$

and an eccentric GW-mergers volumetric rate of

$$R_{\text{IMS,eccentric}} \approx 1 - 10 \times F_{\text{model}}\text{Gpc}^{-3}\text{yr}^{-1}. \quad (55)$$

comparable and consistent with the currently inferred rate of BBH GW-mergers, and consistent with the current no detections of eccentric mergers, given the, still, too low statistics. We do expect, however, a few eccentric mergers to be

detected over the coming few years, once the cumulative number of identified GW-sources is of the order of several hundreds.

We also predict the spin-orbit alignment of the GW mergers from this channel to generally be isotropic. We also predict a close to uniform delay time distribution, with a significant contribution from both early and late type galaxies, and a preference for galaxies with higher velocity dispersions which are more favorable for field interactions with wide TBHs.

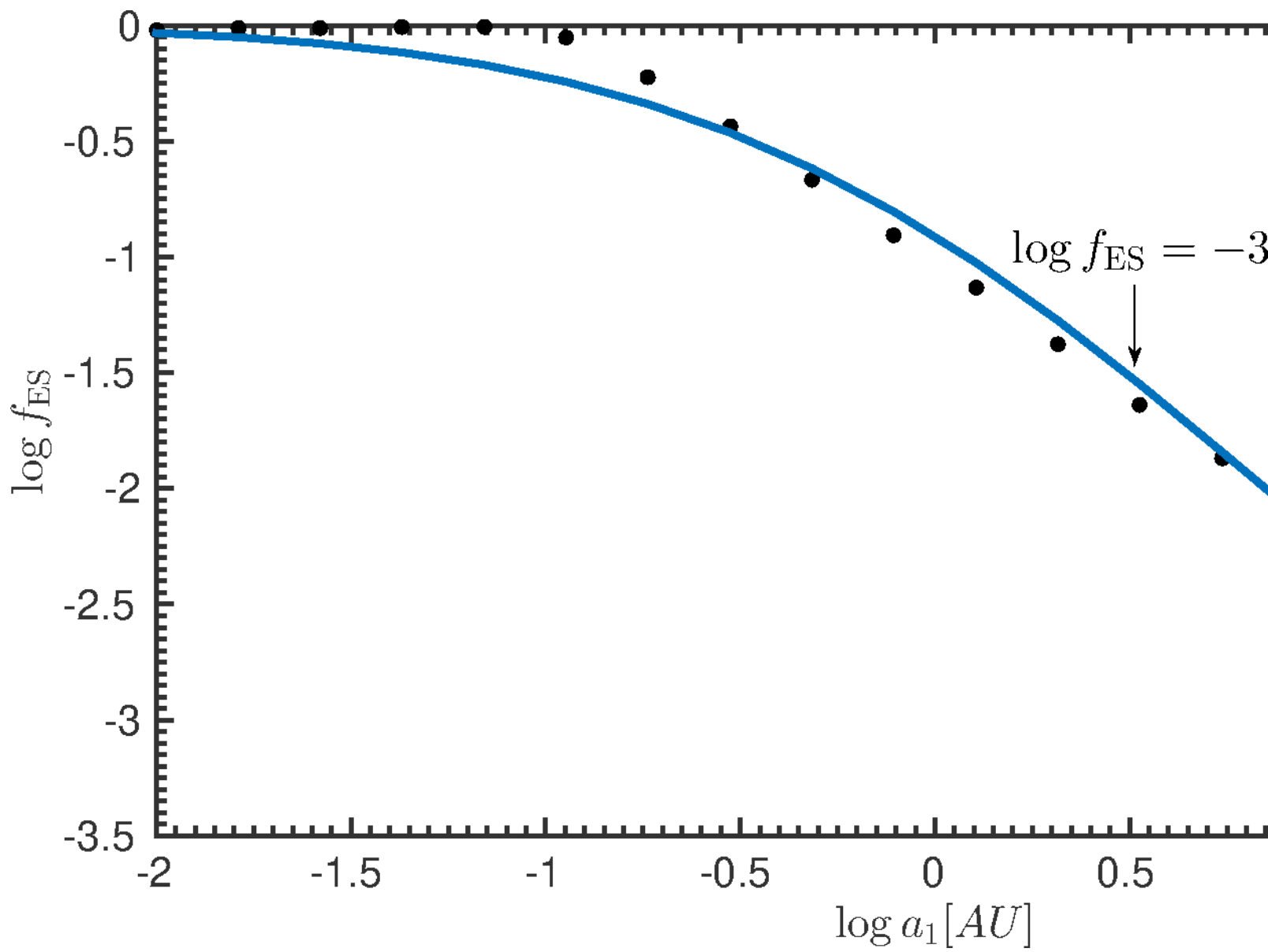
ACKNOWLEDGEMENTS

EM thanks Johan Samsing for helpful and enlightening discussion that lead to this project. HBP acknowledges support from the Kingsley distinguished-visitor program in Caltech, where some of the work has been done.

Data availability The data underlying this article will be shared on reasonable request to the corresponding author.

REFERENCES

- Adams S. M., Kochanek C. S., Gerke J. R., Stanek K. Z., Dai X., 2017, *MNRAS*, **468**, 4968
- Antognini J. M., Shappee B. J., Thompson T. A., Amaro-Seoane P., 2014, *MNRAS*, **439**, 1079
- Antonini F., Perets H. B., 2012, *ApJ*, **757**, 27
- Antonini F., Murray N., Mikkola S., 2014, *ApJ*, **781**, 45
- Antonini F., Chatterjee S., Rodriguez C. L., Morscher M., Pat-tabiraman B., Kalogera V., Rasio F. A., 2016, *ApJ*, **816**, 65
- Antonini F., Toonen S., Hamers A. S., 2017, *ApJ*, **841**, 77
- Bahcall J. N., Hut P., Tremaine S., 1985, *ApJ*, **290**, 15
- Banerjee S., 2018, *MNRAS*, **473**, 909
- Belczynski K., Kalogera V., Bulik T., 2002, *ApJ*, **572**, 407
- Belczynski K., Sadowski A., Rasio F. A., 2004, *ApJ*, **611**, 1068
- Belczynski K., Taam R. E., Kalogera V., Rasio F. A., Bulik T., 2007, *ApJ*, **662**, 504
- Belczynski K., Kalogera V., Rasio F. A., Taam R. E., Zezas A., Bulik T., Maccarone T. J., Ivanova N., 2008, *ApJS*, **174**, 223
- Belczynski K., Repetto S., Holz D. E., O’Shaughnessy R., Bulik T., Berti E., Fryer C., Dominik M., 2016, *ApJ*, **819**, 108
- Dominik M., Belczynski K., Fryer C., Holz D. E., Berti E., Bulik T., Mandel I., O’Shaughnessy R., 2012, *ApJ*, **759**, 52
- Dominik M., et al., 2015, *ApJ*, **806**, 263
- Ertl T., Janka H.-T., Woosley S. E., Sukhbold T., Ugliano M., 2015, preprint, ([arXiv:1503.07522](https://arxiv.org/abs/1503.07522))
- Fragione G., Kocsis B., 2018, *Phys. Rev. Lett.*, **121**, 161103
- Fragione G., Grishin E., Leigh N. W. C., Perets H. B., Perna R., 2019, *MNRAS*, **488**, 47
- Fryer C. L., Woosley S. E., Hartmann D. H., 1999, *ApJ*, **526**, 152
- Hamers A. S., Bar-Or B., Petrovich C., Antonini F., 2018, *ApJ*, **865**, 2
- Hamilton C., Rafikov R. R., 2019, *MNRAS*, **488**, 5512
- Harry G. M., LIGO Scientific Collaboration 2010, *Classical and Quantum Gravity*, **27**, 084006
- Heggie D. C., 1975, *MNRAS*, **173**, 729
- Hernquist L., 1990, *ApJ*, **356**, 359
- Hills J. G., 1975, *AJ*, **80**, 809
- Hills J. G., 1981, *AJ*, **86**, 1730
- Hoang B.-M., Naoz S., Kocsis B., Rasio F. A., Dosopoulou F., 2018, *ApJ*, **856**, 140
- Hut P., Tremaine S., 1985, *AJ*, **90**, 1548
- Igoshev A. P., Perets H. B., 2019, arXiv e-prints,
- Jurić M., et al., 2008, *ApJ*, **673**, 864
- Kaib N. A., Raymond S. N., 2014, *ApJ*, **782**, 60
- Kopparapu R. K., Hanna C., Kalogera V., O’Shaughnessy R., González G., Brady P. R., Fairhurst S., 2008, *ApJ*, **675**, 1459
- Kozai Y., 1962, *AJ*, **67**, 591
- Kroupa P., 2001, *MNRAS*, **322**, 231
- LIGO Scientific Collaboration Virgo Collaboration 2019, *Physical Review X*, **9**, 031040
- Leigh N. W. C., et al., 2018, *MNRAS*, **474**, 5672
- Lidov M. L., 1962, *Planet. Space Sci.*, **9**, 719
- Lightman A. P., Shapiro S. L., 1977, *ApJ*, **211**, 244
- Mandel I., 2016, *MNRAS*, **456**, 578
- Mandel I., de Mink S. E., 2016, *MNRAS*, **458**, 2634
- Mardling R. A., Aarseth S. J., 2001, *MNRAS*, **321**, 398
- Merritt D., 2013, *Classical and Quantum Gravity*, **30**, 244005
- Michaely E., Perets H. B., 2014, *ApJ*, **794**, 122
- Michaely E., Perets H. B., 2016, *MNRAS*, **458**, 4188
- Michaely E., Perets H. B., 2018, *ApJ*, **855**, L12
- Michaely E., Perets H. B., 2019, *ApJ*, **887**, L36
- Moe M., Di Stefano R., 2016, preprint, ([arXiv:1606.05347](https://arxiv.org/abs/1606.05347))
- Naoz S., 2016, *ARA&A*, **54**, 441
- Perets H. B., Kouwenhoven M. B. N., 2012, *ApJ*, **750**, 83
- Peters P. C., 1964, *Physical Review*, **136**, 1224
- Petrovich C., Antonini F., 2017, *ApJ*, **846**, 146
- Repetto S., Davies M. B., Sigurdsson S., 2012, *MNRAS*, **425**, 2799
- Repetto S., Igoshev A. P., Nelemans G., 2017, *MNRAS*, **467**, 298
- Rodriguez C. L., Chatterjee S., Rasio F. A., 2016, *Phys. Rev. D*, **93**, 084029
- Rodriguez C. L., Amaro-Seoane P., Chatterjee S., Kremer K., Rasio F. A., Samsing J., Ye C. S., Zevin M., 2018, *Phys. Rev. D*, **98**, 123005
- Samsing J., D’Orazio D. J., 2018, *MNRAS*, **481**, 5445
- Samsing J., Ramirez-Ruiz E., 2017, *ApJ*, **840**, L14
- Samsing J., MacLeod M., Ramirez-Ruiz E., 2014, *ApJ*, **784**, 71
- Samsing J., MacLeod M., Ramirez-Ruiz E., 2018a, *ApJ*, **853**, 140
- Samsing J., Askar A., Giersz M., 2018b, *ApJ*, **855**, 124
- Sana H., et al., 2014, *ApJS*, **215**, 15
- Silsbee K., Tremaine S., 2017, *ApJ*, **836**, 39
- Stone N. C., Leigh N. W. C., 2019, *Nature*, **576**, 406
- Wen L., 2003, *ApJ*, **598**, 419
- Will C. M., 2014, *Phys. Rev. D*, **89**, 044043
- de Mink S. E., Belczynski K., 2015, *ApJ*, **814**, 58



eccentricity distribution at 10Hz

